

A conservative scheme of drift kinetic electrons for gyrokinetic simulation of kinetic-MHD processes in toroidal plasmas

J. Bao,^{1,2} D. Liu,³ and Z. Lin^{1,a)}

¹*Department of Physics and Astronomy, University of California, Irvine, California 92697, USA*

²*Fusion Simulation Center, Peking University, Beijing 100871, China*

³*College of Physical Science and Technology, Sichuan University, Chengdu 610064, China*

(Received 11 July 2017; accepted 24 August 2017; published online 23 October 2017)

A conservative scheme of drift kinetic electrons for gyrokinetic simulations of kinetic-magnetohydrodynamic processes in toroidal plasmas has been formulated and verified. Both vector potential and electron perturbed distribution function are decomposed into adiabatic part with analytic solution and non-adiabatic part solved numerically. The adiabatic parallel electric field is solved directly from the electron adiabatic response, resulting in a high degree of accuracy. The consistency between electrostatic potential and parallel vector potential is enforced by using the electron continuity equation. Since particles are only used to calculate the non-adiabatic response, which is used to calculate the non-adiabatic vector potential through Ohm's law, the conservative scheme minimizes the electron particle noise and mitigates the cancellation problem. Linear dispersion relations of the kinetic Alfvén wave and the collisionless tearing mode in cylindrical geometry have been verified in gyrokinetic toroidal code simulations, which show that the perpendicular grid size can be larger than the electron collisionless skin depth when the mode wavelength is longer than the electron skin depth. *Published by AIP Publishing.* <https://doi.org/10.1063/1.4995455>

I. INTRODUCTION

The excitation and evolution of macroscopic electromagnetic instabilities in magnetized plasmas often depend on kinetic effects at microscopic scales and the nonlinear coupling of multiple physical processes, which span disparate spatial and temporal scales. For example, the excitation of the neoclassical tearing mode (NTM), the most likely instability leading to disruption in tokamak,¹ depends on the nonlinear interaction of magnetohydrodynamic (MHD) instability, microturbulence, collisional (neoclassical) transport, and energetic particle effects. NTM islands flatten the local pressure profile and modify plasma flow, thus affecting microturbulence and the neoclassical bootstrap current. On the other hand, microturbulence can impact island dynamics by regulating plasma current and electron heat conductivity along and across the magnetic field and by driving sheared flows via Reynolds stress and Maxwell stress. Energetic particles also strongly affect the tearing modes. A fully self-consistent NTM simulation must incorporate nonlinear interactions between resistive MHD tearing modes, neoclassical transport, microturbulence, and energetic particle effects. All these kinetic-MHD processes have characteristic frequencies below ion cyclotron frequency, which can be most efficiently studied by the gyrokinetic simulation model.²⁻⁴

Gyrokinetic particle simulation⁴⁻⁷ has emerged as a powerful tool for studying nonlinear physics of low frequency kinetic-MHD processes thanks to advances in physics models, numerical algorithms, and computing power. In particular, the

formulation of a perturbative (δf) simulation method^{8,9} has drastically reduced particle noises. Nonetheless, electromagnetic gyrokinetic particle simulation incorporating simultaneously ion and electron dynamics is numerically challenging due to the small electron-to-ion mass ratio, especially for the long wavelength modes in high β (ratio of kinetic to magnetic pressure) plasmas.^{10,11} Thus, a split-weight scheme^{12,13} has been developed to analytically calculate the electron adiabatic responses to the parallel electric field, which further reduces electron noises.

However, the parallel electric field can be insignificant for long wavelength shear Alfvén waves with non-tearing parity (such as kinetic ballooning modes and Alfvén eigenmodes), where the electrostatic parallel electric field nearly cancels out with the inductive parallel electric field when the mode polarization is close to the ideal MHD in high- β (ratio of kinetic to magnetic pressure) plasmas. A small error in calculating the electrostatic and vector potentials could result in a large error in the parallel electric field, which could greatly affect the electron dynamics. The problem is worse for the tearing mode, which is driven by a parallel electric field in a narrow resonant layer with a width of an electron collisionless skin depth. The electron responses to this parallel electric field is not adiabatic since $k_{\parallel} \approx 0$. Outside this narrow tearing layer, the parallel electric field is small, and the electron response is close to the ideal MHD response in the form of massless (adiabatic) electrons, which carry a non-resonant current that induces the Alfvén waves. A numerical difficulty is to recover this non-resonant current from the electron distribution function when the parallel electric field is very small in the ideal MHD limit.

Another well-known numerical difficulty in electromagnetic gyrokinetic simulations is that the calculation of the

Note: Paper submitted as part of the Special Topic on Gyrokinetic Particle Simulation: A Symposium in Honor of Wei-li Lee (Guest Editor: Zhihong Lin). The Conference was held at University of California, Irvine, July 18–22, 2016.

^{a)} Author to whom correspondence should be addressed: zhihongl@uci.edu.

inductive parallel electric field requires a time-derivative of the parallel vector potential, an operation often leading to a numerical instability. To avoid this explicit time-derivative operation, a popular practice is to use canonical momentum as an independent velocity variable (p_{\parallel} -formulation), which artificially adds two large terms to the original Ampere law. Analytically, these two terms should cancel exactly with each other. However, a small error in numerically evaluating these two terms in Ampere's law can give rise to a residue that leads to a large error in the parallel vector potential,^{14,15} which is known as the "cancellation problem" in some gyrokinetic particle and continuum codes, which requires sophisticated numerical techniques or reduced physics models.^{15–28} Furthermore, to mitigate the cancellation problem in the electromagnetic simulations, the perturbative (δf) method or the split-weight scheme needs to use a small perpendicular grid size of the collisionless electron skin depth even for simulations of non-tearing modes such as electromagnetic ion temperature gradient (ITG) instability.²⁶

To overcome the difficulties of simultaneously treating the dynamics of ions and electrons in electromagnetic simulations, a reduced fluid-kinetic hybrid electron model^{22–25} was developed by expanding the electron drift kinetic equation using the electron-to-ion mass ratio as a small parameter. In the lowest order, the electron is adiabatic and becomes a massless fluid. The electron kinetic effects are incorporated in the higher order kinetic equation. It is important here to calculate the parallel electric field directly from electron parallel force balance rather than from the cancellation between electrostatic and inductive fields. Another key technique is to calculate the non-resonant current from the adiabatic response by using the parallel vector potential rather than from the electron distribution function that suffers from electron particle noises. This model accurately recovers low frequency plasma dielectric responses and faithfully preserves linear and nonlinear wave-particle resonance for non-tearing modes in the simulations of microturbulence and Alfvén eigenmodes using the gyrokinetic toroidal code (GTC).^{29–39} The maximum numerical efficiency is achieved by overcoming the electron Courant condition and suppressing tearing modes (and associated electron noises). The fluid-kinetic hybrid electron model solves the original Ampere law, which is free from the cancellation problem. Recently, the hybrid model has been extended to incorporate the tearing modes by adding the resistivity to the electron momentum equation for the resistive tearing mode⁴⁰ and by implementing the finite-mass electron fluid model⁴¹ for the collisionless tearing mode.⁴²

Nonetheless, it is desirable to develop a unified formulation that solves the exact electron drift kinetic equation to incorporate low frequency electromagnetic fluctuations with both tearing parity and non-tearing parity on the same footing in the gyrokinetic simulations of nonlinear interactions of multiple kinetic-MHD processes in high- β plasmas. This aim builds on our recent work,⁴³ where we show that the perturbed electron density and current measured from kinetic markers in conventional gyrokinetic simulations do not satisfy the electron continuity equation in the conventional δf scheme due to the electron particle noises. Consequently, the electrostatic potential calculated from the density and the

parallel vector potential calculated from the current are not consistent with each other, which results in an unphysically large parallel electric field. This inconsistency is the primary cause of the well-known numerical difficulty of electromagnetic δf simulation of long wavelength MHD modes with kinetic electrons as shown by our theoretical error analysis.⁴³ To overcome this inconsistency problem, only the highest order moment (either electron flow or pressure) required to close the electron fluid system is calculated by using the distribution function, and other lower order moments are calculated from conservative moment equations of the drift kinetic equation. This new electron scheme, which is referred to as a "conservative scheme,"⁴³ solves the exact drift kinetic equation. For example, our scheme in the p_{\parallel} -formulation uses the continuity equation to time advance the electron density perturbation, and only the perturbed canonical flow is calculated from the perturbed distribution function.⁴³ In the v_{\parallel} -formulation (using parallel velocity as an independent velocity variable), we need to use both electron continuity and momentum equations, and the electron kinetic effects come into the system through the electron pressure.

In this work, the original fluid-kinetic hybrid electron model is extended to solving the exact drift kinetic electron model using the conservative scheme⁴³ in the v_{\parallel} -formulation. In this new conservative scheme, the electron density perturbation is calculated from the continuity equation, the electron flow is calculated from the vector potential by inverting Ampere's law, and the vector potential is calculated from Ohm's law. Only the highest order moment, i.e., electron pressure, is calculated from the guiding center distribution function, which is used to close the system. The electron perturbed distribution function δf is decomposed into adiabatic part and non-adiabatic part $\delta f = \delta f_a + \delta h$. We further separate the parallel vector potential A_{\parallel} into adiabatic part and non-adiabatic part $A_{\parallel} = \delta A_{\parallel}^A + A_{\parallel}^{NA}$. The adiabatic vector potential δA_{\parallel}^A and the adiabatic distribution δf_a are defined and analytically solved self-consistently with each other. The non-adiabatic perturbed distribution function δh can then be calculated in the simulation. By using the total Ohm law for A_{\parallel} integrated from the drift kinetic equation and the analytic solution of δA_{\parallel}^A , Ohm's law for solving A_{\parallel}^{NA} can be derived and solved in the simulation. In summary, our conservative scheme solves the adiabatic parallel electric field directly from the electron adiabatic response. The non-adiabatic parallel electric field is solved from Ohm's law using the electron non-adiabatic distribution function, which is free from the cancellation problem. The perturbed density and parallel flow are numerically conserved thanks to the use of the continuity equation and Ohm's law, which brings numerical stability for long time simulation.

The conservative scheme guarantees the conservation properties of electron perturbed density and parallel flow and thus the consistency between the electrostatic potential and parallel vector potential. Since only the non-adiabatic electron response is calculated by using particles, our conservative scheme minimizes the electron particle noise like the split-weight scheme. Furthermore, the field equation for adiabatic vector potential is free from the cancellation problem, while the generalized Ohm law is only used to solve the non-

adiabatic vector potential by using the non-adiabatic electron response, which mitigates the cancellation problem. We will show that the perpendicular grid size can be much larger than the electron skin depth for simulations of long wavelength modes. The linear dispersion relations of the kinetic Alfvén wave (KAW) in uniform plasmas and the collisionless tearing mode in cylindrical geometry have been verified in simulations using GTC. This conservative scheme can faithfully capture the tearing mode physics and will be utilized for the gyrokinetic simulation of the nonlinear interaction of multiple kinetic-MHD processes in toroidal plasmas ranging from the micro-tearing mode⁴⁵ to the neoclassical tearing mode.

This paper is organized as follows: The electromagnetic gyrokinetic model with $v_{||}$ formulation and the perturbative δf simulation method are described in Sec. II. In Sec. III, we formulate the conservative scheme of the drift kinetic electron model for nonlinear electromagnetic simulations in toroidal geometry. The verifications of this scheme for simulations of the kinetic Alfvén wave and the collisionless tearing mode are shown in Sec. IV. Conclusions are drawn in Sec. V.

II. ELECTROMAGNETIC GYROKINETIC SIMULATION MODEL

A. Nonlinear gyrokinetic equations and field equations

The gyrokinetic model has been widely used to study low frequency waves and instabilities in tokamak plasmas. The following gyrokinetic ordering is adopted in this paper:

$$\frac{\omega}{\Omega_i} \sim \frac{\delta f}{f} \sim \frac{e\phi}{T} \sim \frac{\delta B}{B_0} \sim k_{||}\rho_i \sim O(\varepsilon_g) \ll 1,$$

where ω and $\Omega_i = eB_0/cm_i$ are the physical mode frequency and ion cyclotron frequency, m_i is the ion mass, $v_{thi} = \sqrt{T/m_i}$ is the ion thermal velocity, $\rho_i = v_{thi}/\Omega_i$ is the ion gyroradius, δf and f are the perturbed and total particle distributions, ϕ and δB are the perturbed electrostatic potential and the perturbed magnetic field, and $k_{||}$ is the parallel wave vector. This gyrokinetic ordering does not assume short perpendicular wavelengths and thus can be used for simulations of long wavelength modes in the toroidal geometry. This ordering can be extended to allow the equilibrium gradient scale length on the order of the perpendicular wavelength.⁴⁴

The following gyrokinetic Vlasov equation describes the gyrocenter dynamics by using gyrocenter position \mathbf{R} , magnetic moment μ , and parallel velocity $v_{||}$ as independent variables in the five dimensional phase space²

$$\left(\frac{\partial}{\partial t} + \dot{\mathbf{R}} \cdot \nabla + \dot{v}_{||} \frac{\partial}{\partial v_{||}} \right) f_{\alpha}(\mathbf{R}, v_{||}, \mu, t) = 0, \quad (1)$$

$$\dot{\mathbf{R}} = v_{||}\mathbf{b}_0 + v_{||} \frac{\delta \mathbf{B}}{B_0} + \bar{\mathbf{v}}_E + \mathbf{v}_d + \mathbf{v}_{NL}, \quad (2)$$

$$\dot{v}_{||} = -\frac{1}{m_{\alpha} B_{||}^*} \cdot (Z_{\alpha} \nabla \bar{\phi} + Z_{\alpha} \nabla \psi_{NL} + \mu \nabla B_0) - \frac{Z_{\alpha}}{cm_{\alpha}} \frac{\partial \bar{A}_{||}}{\partial t}, \quad (3)$$

where Z_{α} , m_{α} , and f_{α} represent the charge, mass, and distribution of $\alpha = i, e$ particle species, respectively. $A_{||}$ is the perturbed parallel vector potential, $\mathbf{B}_0^* = \mathbf{B}_0 + (B_0 v_{||}/\Omega_{\alpha}) \nabla \times \mathbf{b}_0$,

$B_{||}^* = \mathbf{b}_0 \cdot \mathbf{B}_0^*$, $\delta \mathbf{B} = \nabla \times (\bar{A}_{||} \mathbf{b}_0)$, and $\mathbf{B}^* = \mathbf{B}_0^* + \delta \mathbf{B}$. The nonlinear potential $Z_{\alpha} \psi_{NL} = \frac{\mu}{2B_0} |\delta \mathbf{B}|^2 - \frac{m_{\alpha}}{2} |\mathbf{v}_E + v_{||} \frac{\delta \mathbf{B}}{B_0}|^2$ is given in the drift kinetic limit.² $\Omega_{\alpha} = \frac{Z_{\alpha} B_0}{cm_{\alpha}}$ is the cyclotron frequency. The overbar $\overline{(\cdots)} = \frac{1}{2\pi} \int d\mathbf{x} d\zeta (\cdots) \delta(\mathbf{R} + \boldsymbol{\rho}_{\alpha} - \mathbf{x})$ represents gyroaverage, ζ is the gyrophase angle, \mathbf{x} is the particle position, and $\boldsymbol{\rho}_{\alpha} = \frac{\mathbf{b}_0 \times \mathbf{v}_{\perp}}{\Omega_{\alpha}}$ is the gyroradius. For the drift kinetic electron, the gyro-average can be removed, and $\mathbf{R} = \mathbf{x}$ in Eqs. (1)–(3). \mathbf{v}_E and \mathbf{v}_{NL} are the perturbed $E \times B$ drift due to the electrostatic potential and nonlinear potential, respectively, and \mathbf{v}_d is the magnetic drift

$$\bar{\mathbf{v}}_E = \frac{c}{B_{||}^*} \mathbf{b}_0 \times \nabla \bar{\phi},$$

$$\mathbf{v}_{NL} = \frac{c}{B_{||}^*} \mathbf{b}_0 \times \nabla \psi_{NL},$$

and

$$\mathbf{v}_d = \frac{cm_{\alpha} v_{||}^2}{Z_{\alpha} B_{||}^*} \mathbf{b}_0 \times (\mathbf{b}_0 \cdot \nabla \mathbf{b}_0) + \frac{c\mu}{Z_{\alpha} B_{||}^*} \mathbf{b}_0 \times \nabla B_0.$$

The appearance of $B_{||}^*$ ensures that the gyrocenter equations of motion preserve the Hamiltonian structure and satisfy Liouville's theorem²

$$\frac{\partial f_{\alpha} B_{||}^*}{\partial t} + \nabla \cdot (\dot{\mathbf{R}} f_{\alpha} B_{||}^*) + \frac{\partial}{\partial v_{||}} (\dot{v}_{||} f_{\alpha} B_{||}^*) = 0. \quad (4)$$

Eq. (4) in the conservative form is equivalent to Eqs. (1)–(3).

The electrostatic potential ϕ is solved by the gyrokinetic Poisson equation

$$\frac{Z_i^2 n_{i0}}{T_{i0}} (\phi - \tilde{\phi}) = Z_i \bar{n}_i - n_e, \quad (5)$$

where $\tilde{\phi}(\mathbf{x}, t) = \frac{1}{n_i} \int d\mathbf{v} f_{i0}(\mathbf{R}, v_{||}, \mu, t) \bar{\phi}(\mathbf{R}, t)$ is the second gyrophase-averaged potential, f_{i0} is the ion equilibrium distribution, $\bar{n}_i(\mathbf{x}, t) = \int d\mathbf{v} f_i(\mathbf{R}, v_{||}, \mu, t)$ and $n_e(\mathbf{x}, t) = \int d\mathbf{v} f_e(\mathbf{x}, v_{||}, \mu, t)$ are the gyrophase-averaged ion and electron densities, and $\int d\mathbf{v} = \frac{2\pi}{m_i} \int B_{||}^* dv_{||} \int d\mu \frac{1}{2\pi} \int \delta(\mathbf{R} + \boldsymbol{\rho}_{\alpha} - \mathbf{x}) d\mathbf{R} d\zeta$. The electrostatic potential ϕ , ion density \bar{n}_i , and electron density n_e contain both zonal and non-zonal components. We can solve Eq. (5) for both zonal and non-zonal components together or we can solve them separately.

The parallel vector potential $A_{||}$ is solved by the parallel Ampere law

$$\nabla_{\perp}^2 A_{||} = -\frac{4\pi}{c} (\bar{J}_{||i} + J_{||e}), \quad (6)$$

where $\bar{J}_{||i}(\mathbf{x}, t) = Z_i \int v_{||} d\mathbf{v} f_i(\mathbf{X}, v_{||}, \mu, t)$ and $J_{||e}(\mathbf{x}, t) = q_e \int v_{||} d\mathbf{v} f_e(\mathbf{x}, v_{||}, \mu, t)$.

Equations (1)–(3), (5), and (6) form a closed system with the $v_{||}$ -formulation, sometime called ‘‘symplectic representation,’’ for electromagnetic gyrokinetic simulations of low frequency waves and instabilities in magnetized plasmas. The perpendicular Ampere law can be added to incorporate the compressional magnetic perturbations in the above model.⁴⁶

B. Perturbative δf simulation scheme

To reduce particle noises, a perturbative (δf) simulation scheme^{8,9} has been developed and successfully exercised in gyrokinetic simulations by splitting the total distribution function into the equilibrium and perturbed parts $f_\alpha = f_{\alpha 0} + \delta f_\alpha$. Only the perturbed distribution function δf_α is dynamically calculated in the simulation, which reduces the numerical noise by a factor of $(\delta f_\alpha/f_\alpha)^2$. The equilibrium distribution $f_{\alpha 0}$ is defined as

$$L_0 f_{\alpha 0} = 0, \quad (7)$$

where $L_0 = \frac{\partial}{\partial t} + (v_{\parallel} \mathbf{b}_0 + \mathbf{v}_d) \cdot \nabla - \frac{\mu}{m_\alpha B_{\parallel}^*} \mathbf{B}_0^* \cdot \nabla B_0 \frac{\partial}{\partial v_{\parallel}}$ is the equilibrium propagator. The equilibrium distribution function $f_{\alpha 0}$ in the toroidal geometry is a neoclassical solution to Eq. (7).⁴⁷ In the δf simulation method, the neoclassical solution $f_{\alpha 0}$ to Eq. (7) is implicitly built-in but can be solved in the gyrokinetic simulation using the δf method.^{48,49} The equilibrium distribution function $f_{\alpha 0}$ then appears as a source for the perturbed δf_α equation, where $f_{\alpha 0}$ can then be approximated as a shifted Maxwellian as routinely used in the analytic theory and turbulence simulation: $f_{\alpha 0} = n_{\alpha 0} \left(\frac{m_\alpha}{2\pi T_{\alpha 0}} \right)^{3/2} \exp \left[-\frac{m_\alpha (v_{\parallel} - u_{\parallel \alpha 0})^2 + 2\mu B_0^*}{2T_{\alpha 0}} \right]$, where $u_{\parallel \alpha 0}$ is the parallel equilibrium flow of each species, and the equilibrium Ampere law is satisfied: $Z_i n_{i0} u_{\parallel i0} - e n_{e0} u_{\parallel e0} = \frac{c}{4\pi} \mathbf{b}_0 \cdot \nabla \times \mathbf{B}_0$, where $n_{\alpha 0}$ is the equilibrium density and $T_{\alpha 0}$ is the equilibrium temperature of each species. The effects of neoclassical transport on microturbulence can be incorporated by adding the neoclassical source term in the δf_α equation.

Using Eq. (7) to subtract Eq. (1), the equation of δf_α can be derived as

$$L \delta f_\alpha = -(\delta L_1 + \delta L_2) f_{\alpha 0}, \quad (8)$$

where $L = \frac{\partial}{\partial t} + \dot{\mathbf{R}} \cdot \nabla + \dot{v}_{\parallel} \frac{\partial}{\partial v_{\parallel}}$ is the total propagator and δL_1 and δL_2 are the linear and nonlinear perturbed propagators

$$\begin{aligned} \delta L_1 &= \left(v_{\parallel} \frac{\delta \mathbf{B}}{B_{\parallel}^*} + \overline{\mathbf{v}_E} \right) \cdot \nabla \\ &\quad - \left[\frac{\mu}{m_\alpha B_{\parallel}^*} \delta \mathbf{B} \cdot \nabla B_0 + \frac{Z_\alpha}{m_\alpha} \left(\frac{\mathbf{B}_0^*}{B_{\parallel}^*} \cdot \nabla \bar{\phi} + \frac{1}{c} \frac{\partial \overline{A_{\parallel}}}{\partial t} \right) \right] \frac{\partial}{\partial v_{\parallel}}, \\ \delta L_2 &= \mathbf{v}_{\text{NL}} \cdot \nabla - \frac{Z_\alpha}{m_\alpha B_{\parallel}^*} \delta \mathbf{B} \cdot \nabla \bar{\phi} \frac{\partial}{\partial v_{\parallel}} - \frac{Z_\alpha \mathbf{B}_0^*}{m_\alpha B_{\parallel}^*} \cdot \nabla \psi_{\text{NL}} \frac{\partial}{\partial v_{\parallel}}. \end{aligned}$$

Here, we only keep nonlinear terms up to the second order in δL_2 .

In the simulation, we can rewrite Eq. (8) by defining the particle weight as $w_\alpha = \delta f_\alpha / f_\alpha$

$$\begin{aligned} \frac{dw_\alpha}{dt} &= (1 - w_\alpha) \left[- \left(v_{\parallel} \frac{\delta \mathbf{B}}{B_{\parallel}^*} + \overline{\mathbf{v}_E} + \mathbf{v}_{\text{NL}} \right) \cdot \frac{\nabla f_{\alpha 0}}{f_{\alpha 0}} \right. \\ &\quad + \left(\frac{\delta \mathbf{B}}{B_{\parallel}^*} \cdot \nabla B_0 + \frac{Z_\alpha \mathbf{B}_0^*}{m_\alpha B_{\parallel}^*} \cdot \nabla \bar{\phi} + \frac{Z_\alpha}{c} \frac{\partial \overline{A_{\parallel}}}{\partial t} + \frac{Z_\alpha \mathbf{B}_0^*}{m_\alpha B_{\parallel}^*} \cdot \nabla \psi_{\text{NL}} \right) \\ &\quad \left. \times \frac{1}{m_\alpha f_{\alpha 0}} \frac{\partial f_{\alpha 0}}{\partial v_{\parallel}} \right]. \quad (9) \end{aligned}$$

In principles, Eqs. (1)–(3), (5), (6), and (9) can be used as a closed system for the perturbative δf simulations. However, due to the small electron-ion mass ratio, it is difficult to apply these equations directly for the electromagnetic simulations, especially for the long wavelength MHD modes. The time derivative of the parallel vector potential $\partial A_{\parallel} / \partial t$ in the v_{\parallel} -formulation is also difficult to evaluate by a finite difference method. To overcome these difficulties, in Sec. III, we will formulate the conservative scheme of the drift kinetic electron with the v_{\parallel} formulation for the gyrokinetic simulations of kinetic-MHD processes in toroidal geometry.

III. CONSERVATIVE SCHEME FOR DRIFT KINETIC ELECTRON

In this section, the subscript “e” in most of the electron quantities is omitted for simplicity since our formulation of the conservative scheme is only for drift kinetic electrons. To simplify electron equations for our conservative scheme, we use the following auxiliary ordering, which can be relaxed if necessary,

$$\frac{k_{\parallel}}{k_{\perp}} \sim \frac{1}{k_{\perp} L} \sim O(\varepsilon) < 1,$$

where k_{\perp} is the perpendicular wave vector and L is the plasma equilibrium scale length $L \sim (L_n = \nabla \ln n, L_T = \nabla \ln T, L_B = \nabla \ln B_0)$ (T is the plasma temperature, n is the electron density, and B_0 is the equilibrium magnetic field). The small parameter $\varepsilon = a/R$ is the inverse aspect ratio, where a is the minor radius and R is the major radius. We keep all linear terms of the electron drift kinetic equation (i.e., both tearing parity and non-tearing parity) and nonlinear terms up to the order $O(\varepsilon \varepsilon_g)$ in Eq. (8). The term related to the nonlinear potential ψ_{NL} in Eq. (8) is the order $O(\varepsilon_g^2 \varepsilon)$ and thus dropped for both ion and electron species since $|\psi_{\text{NL}}|/|\phi| \sim O(\varepsilon_g)$. This ordering is valid for long wavelength MHD modes with a low toroidal mode number.

The electrostatic potential ϕ is separated into the non-zonal part $\delta \phi$ and the zonal part (flux-surface averaged part) $\langle \phi \rangle$ as

$$\phi = \delta \phi + \langle \phi \rangle,$$

where $\langle \dots \rangle = \frac{\int (\dots) J d\theta d\zeta}{\int J d\theta d\zeta}$ represents the flux surface averaging,

θ and ζ are the poloidal and toroidal angles in magnetic coordinates, and J is the Jacobian. The zonal and non-zonal components can be solved by Eq. (5) together or solved separately by using the non-zonal and zonal solvers in practice due to the large difference of the amplitude between non-zonal and zonal components in nonlinear simulation.^{1,24,36} The parallel vector potential A_{\parallel} consists of the adiabatic part δA_{\parallel}^A and the non-adiabatic part $A_{\parallel}^{\text{NA}}$ as

$$A_{\parallel} = \delta A_{\parallel}^A + A_{\parallel}^{\text{NA}}.$$

The adiabatic part δA_{\parallel}^A only contains the non-zonal component associated with electron adiabatic responses and the non-resonant current as in the fluid-kinetic hybrid electron model.²² The non-adiabatic part $A_{\parallel}^{\text{NA}}$ contains both the zonal

component $\langle A_{\parallel}^{NA} \rangle$ and non-zonal component $\delta A_{\parallel}^{NA}$ due to electron non-adiabatic responses and nonlinear ponderomotive forces.

The electron distribution function consists of the equilibrium and perturbed parts as $f = f_0 + \delta f$, which are described by Eqs. (7) and (8), respectively. The equilibrium distribution provides the equilibrium density $n_0 = \int f_0 d\mathbf{v}$, which does not evolve in the simulation. The perturbed distribution produces perturbed density $\delta n = \int \delta f d\mathbf{v}$, which evolves in the simulation. We further separate the perturbed distribution δf into the adiabatic response δf_a and non-adiabatic response δh as $\delta f = \delta f_a + \delta h$.

The adiabatic vector potential δA_{\parallel}^A is defined as

$$\frac{\partial \delta A_{\parallel}^A}{\partial t} = c \mathbf{b}_0 \cdot \nabla \delta \phi_{ind}, \quad (10)$$

where the non-zonal field $\delta \phi_{ind}$ is defined as

$$\frac{e \delta \phi_{ind}}{T_0} = \frac{\delta n - \langle \delta n \rangle}{n_0} - \frac{e \delta \phi}{T_0} - \frac{\partial n_0}{\partial \psi} \frac{\delta \psi^A}{n_0} - \frac{\partial n_0}{\partial \alpha} \frac{\delta \alpha^A}{n_0}, \quad (11)$$

where perturbed electron density is separated into a zonal part $\langle \delta n \rangle$ and a non-zonal part $\delta n - \langle \delta n \rangle$, ψ is the poloidal flux, and $\alpha = q(\psi)\theta - \zeta$ is the magnetic field line label. $\delta \psi^A$ and $\delta \alpha^A$ are the perturbed quantities. Note that we use electron non-zonal density perturbation to define the adiabatic vector potential through Eqs. (10) and (11).

The adiabatic magnetic perturbation $\delta \mathbf{B}^A$ is defined as

$$\delta \mathbf{B}^A = \nabla \times (\delta A_{\parallel}^A \mathbf{b}_0). \quad (12)$$

Meanwhile, we can write the equilibrium magnetic field and adiabatic magnetic perturbation using the Clebsch representation

$$\mathbf{B}_0 = \nabla \psi_0 \times \nabla \alpha_0 \quad (13)$$

and

$$\delta \mathbf{B}^A = \nabla \psi_0 \times \nabla \delta \alpha^A + \nabla \delta \psi^A \times \nabla \alpha_0. \quad (14)$$

From Eqs. (10), (12)–(14), we obtain the equations for $\delta \psi^A$ and $\delta \alpha^A$

$$\frac{\partial \delta \psi^A}{\partial t} = -c \frac{\partial \delta \phi_{ind}}{\partial \alpha_0}, \quad (15)$$

$$\frac{\partial \delta \alpha^A}{\partial t} = c \frac{\partial \delta \phi_{ind}}{\partial \psi_0}. \quad (16)$$

The adiabatic distribution δf_a is defined by the following equation:

$$\begin{aligned} v_{\parallel} \mathbf{b}_0 \cdot \nabla \delta f_a = & -v_{\parallel} \frac{\delta \mathbf{B}^A}{B_0} \cdot \nabla f_0 \Big|_{\mu} - \left[\frac{\mu}{B_0} \delta \mathbf{B}^A \cdot \nabla B_0 \right. \\ & \left. + q_e \mathbf{b}_0 \cdot \nabla (\delta \phi + \delta \phi_{ind}) \right] \frac{v_{\parallel}}{T_{e0}} f_0. \end{aligned} \quad (17)$$

Using Eqs. (13) and (14), we can solve Eq. (17) and derive δf_a as

$$\delta f_a = \frac{e(\delta \phi + \delta \phi_{ind})}{T_0} f_0 + \frac{\partial f_0}{\partial \psi_0} \Big|_{v_{\perp}} \delta \psi^A + \frac{\partial f_0}{\partial \alpha_0} \Big|_{v_{\perp}} \delta \alpha^A. \quad (18)$$

Integrating Eq. (18) in the velocity space and defining the adiabatic density response $\delta n_a = \int \delta f_a d\mathbf{v}$, we have

$$\frac{\delta n_a}{n_0} = \frac{e(\delta \phi_{ind} + \delta \phi)}{T_0} + \frac{\partial n_0}{\partial \psi} \frac{\delta \psi^A}{n_0} + \frac{\partial n_0}{\partial \alpha} \frac{\delta \alpha^A}{n_0}. \quad (19)$$

We note that Eq. (19) indicates that $\langle \delta n_a \rangle = 0$. From Eqs. (11) and (19), we have

$$\delta n = \delta n_a + \langle \delta n \rangle. \quad (20)$$

Equation (20) indicates that the adiabatic response δf_a contributes to all non-zonal density perturbation, and the non-adiabatic response δh contributes to all zonal density perturbation, i.e., $\int \delta h d\mathbf{v} = \langle \delta n \rangle$. Note that although δh does not contribute to non-zonal density perturbation, it contributes to higher order non-zonal moments such as perturbed flow and pressure. We note that Eqs. (10) and (18) ensure that the adiabatic vector potential δA_{\parallel}^A and the adiabatic distribution δf_a are defined and analytically solved self-consistently with each other, an important consistency absent in the split-weight scheme where the adiabatic response is defined by using the total vector potential.

In order to calculate the total perturbed density δn , we take the moment of Eq. (4) to obtain the electron continuity equation as

$$\begin{aligned} \frac{\partial \delta n}{\partial t} + \nabla \cdot \left[n_0 \left(\delta u_{\parallel e} \mathbf{b}_0 + \mathbf{V}_E + u_{\parallel 0} \frac{\delta \mathbf{B}}{B_0} \right) \right. \\ \left. + \frac{1}{T_0} (\delta P_{\perp} \mathbf{V}_g + \delta P_{\parallel} \mathbf{V}_c) + \frac{n_0 \delta u_{\parallel e}}{B_0} \delta \mathbf{B} + \delta n \mathbf{V}_E \right] = 0, \end{aligned} \quad (21)$$

where the equilibrium part is removed by using Eq. (7). $\delta u_{\parallel e}$ and $u_{\parallel 0}$ are the perturbed and equilibrium parallel velocities of the electron guiding center, and δP_{\parallel} and δP_{\perp} are the perturbed parallel and perpendicular pressures of the electron guiding center. $\mathbf{V}_E = c \mathbf{b}_0 \times \nabla \phi / B_0$ is the $E \times B$ drift, $\mathbf{V}_c = \frac{c T_0}{q_e B_0} \mathbf{b}_0 \times (\mathbf{b}_0 \cdot \nabla \mathbf{b}_0)$, and $\mathbf{V}_g = \frac{c T_0}{q_e B_0} \mathbf{b}_0 \times \nabla B_0$. $\delta \mathbf{B} = \delta \mathbf{B}^A + \delta \mathbf{B}^{NA}$ is the total magnetic perturbation, and $\delta \mathbf{B}^{NA} = \nabla \times (A_{\parallel}^{NA} \mathbf{b}_0)$ is the non-adiabatic part of the magnetic perturbation. The continuity equation [Eq. (21)] together with Ampere's law and the quasi-neutrality condition can recover the MHD vorticity equation in uniform plasmas.⁵²

The values of $\delta u_{\parallel e}$, δP_{\parallel} , and δP_{\perp} are required to evolve Eq. (21). The $\delta u_{\parallel e}$ term can be calculated by inverting Ampere's law Eq. (6) as

$$\delta u_{\parallel e} = \frac{c}{4\pi e n_0} \nabla_{\perp}^2 A_{\parallel} + \frac{Z_i}{e} \delta \bar{u}_{\parallel i}. \quad (22)$$

Here, we use the original Ampere law to derive the parallel electron flow $\delta u_{\parallel e}$. The adiabatic part of the parallel vector potential δA_{\parallel}^A is solved analytically by Eqs. (10) and (11), and the non-adiabatic part of the parallel vector potential A_{\parallel}^{NA} is solved from the non-adiabatic electron response δh , which will be described later. This method is free from the cancellation problem and greatly improves the accuracy of calculating the parallel electric field, especially for the long wavelength modes.

The electron parallel and perpendicular pressures consist of adiabatic and non-adiabatic parts as

$$\delta P_{\parallel} = \int_{DK} m_e v_{\parallel}^2 (\delta f_a + \delta h) \mathbf{d}\mathbf{v} = \delta P_{\parallel}^A + \delta P_{\parallel}^{NA},$$

$$\delta P_{\perp} = \int_{DK} \mu B_0 (\delta f_a + \delta h) \mathbf{d}\mathbf{v} = \delta P_{\perp}^A + \delta P_{\perp}^{NA}.$$

We take the moment of Eq. (18) to get the adiabatic electron pressures as

$$\delta P_{\parallel}^A = en_0 (\delta \phi + \delta \phi_{ind}) + \frac{\partial(n_0 T_0)}{\partial \psi_0} \delta \psi^A + \frac{\partial(n_0 T_0)}{\partial \alpha_0} \delta \alpha^A, \quad (23)$$

$$\delta P_{\perp}^A = en_0 (\delta \phi + \delta \phi_{ind}) + \frac{\partial(n_0 T_0)}{\partial \psi_0} \delta \psi^A + \frac{\partial(n_0 T_0)}{\partial \alpha_0} \delta \alpha^A. \quad (24)$$

The non-adiabatic electron pressures are calculated from the kinetic electron response as

$$\delta P_{\parallel}^{NA} = \int m_e v_{\parallel}^2 \delta h \mathbf{d}\mathbf{v}, \quad (25)$$

$$\delta P_{\perp}^{NA} = \int \mu B_0 \delta h \mathbf{d}\mathbf{v}. \quad (26)$$

When removing the non-adiabatic parts of the parallel vector potential and electron responses, Eqs. (10)–(12), (15), (16), and (21)–(24) form a massless fluid electron model, which is identical to the lowest order adiabatic electron in the fluid-kinetic hybrid electron model.^{22–25}

Next, we formulate the equations for the non-adiabatic kinetic electron response δh and non-adiabatic parallel vector potential A_{\parallel}^{NA} . Using the relation $\delta f = \delta f_a + \delta h$ and Eq. (8), the equation for the non-adiabatic electron response δh can be written as

$$L\delta h = \underbrace{-\delta L_1 f_0 - L_0 \delta f_a}_{\{I\}} - \underbrace{\delta L_2 f_0 - (\delta L_1 + \delta L_2) \delta f_a}_{\{II\}}, \quad (27)$$

where term {I} is linear and term {II} is nonlinear.

Defining the weight function as $w_e = \delta h/f$, one can write the electron weight equation for the electron non-adiabatic response as

$$\frac{dw_e}{dt} = \frac{1 - w_e}{1 + \delta f_a/f_0} [-\delta L_1 f_0 - L_0 \delta f_a - \delta L_2 f_0 - (\delta L_1 + \delta L_2) \delta f_a]. \quad (28)$$

By using the relations of Eqs. (18)–(20), the equation for the time derivative of the adiabatic response $\partial \delta f_a / \partial t$ can be obtained as

$$\begin{aligned} \frac{1}{f_0} \frac{\partial \delta f_a}{\partial t} &= \frac{1}{n_0} \left(\frac{\partial \delta n}{\partial t} - \frac{\partial \langle \delta n \rangle}{\partial t} \right) + \frac{1}{f_0} \frac{\partial f_0}{\partial T_0} \frac{\partial T_0}{\partial \psi_0} \Big|_{v_{\perp}} \frac{\partial \delta \psi^A}{\partial t} \\ &+ \frac{1}{f_0} \frac{\partial f_0}{\partial T_0} \frac{\partial T_0}{\partial \alpha_0} \Big|_{v_{\perp}} \frac{\partial \delta \alpha^A}{\partial t}, \end{aligned} \quad (29)$$

which is required in evolving Eq. (28). The time derivative of the adiabatic response $\partial \delta f_a / \partial t$ can be calculated from Eqs. (15), (16), and (21) easily. In contrast, the time derivative needs to be solved from a higher order moment equation in the split-weight scheme.^{13,26}

In order to close the system, we can solve the non-adiabatic vector potential A_{\parallel}^{NA} using Ohm's law. To obtain Ohm's law, we need the electron momentum equation, which can be integrated from the electron drift kinetic equation [Eq. (4)] in the conservative form,

$$\begin{aligned} n_0 \frac{\partial \delta u_{\parallel e}}{\partial t} + \nabla \cdot [n_0 \delta u_{\parallel e} (\mathbf{V}_E + 3\mathbf{V}_c + \mathbf{V}_g) + n_0 u_{\parallel 0} \mathbf{V}_E] \\ + \frac{q_e}{m_e} n_0 \left[\left(\mathbf{b}_0 + \frac{\delta \mathbf{B}}{B_0} \right) \cdot \nabla \phi + \frac{1}{c} \frac{\partial A_{\parallel}}{\partial t} \right] \\ + \frac{1}{m_e} \nabla \cdot \left[\delta P_{\parallel} \left(\mathbf{b}_0 + \frac{\delta \mathbf{B}}{B_0} \right) + P_{\parallel 0} \frac{\delta \mathbf{B}}{B_0} \right] \\ + \frac{1}{m_e} \left(\frac{P_{\perp 0}}{B_0^2} \delta \mathbf{B} \cdot \nabla B_0 + \frac{\delta P_{\perp}}{B_0} \mathbf{b}_0 \cdot \nabla B_0 \right) = 0, \end{aligned} \quad (30)$$

where we only keep the terms up to the second order $O(\varepsilon_g^2)$ and make a closure and truncation on the parallel energy fluxes: $\int m_e v_{\parallel}^3 \delta f \mathbf{d}\mathbf{v} = n_0 T_0 \delta u_{\parallel e}$ and $\int \mu v_{\parallel} B_0 \delta f \mathbf{d}\mathbf{v} = 3n_0 T_0 \delta u_{\parallel e}$. The truncated term is $\int \nabla \cdot [v_{\parallel} \mathbf{b}_0 B_{\parallel}^* \delta f] v_{\parallel} \mathbf{d}\mathbf{v}$, which is much smaller than the leading order term $\int \nabla \cdot [v_{\parallel} \mathbf{b}_0 B_{\parallel}^* \delta f] v_{\parallel} \mathbf{d}\mathbf{v}$. Here, we note that Eq. (30) with closure and truncation is only used below to derive Ohm's law for the non-adiabatic vector potential. Equation (30) is not used to calculate the electron parallel flow $\delta u_{\parallel e}$, which is calculated by using the exact Ampere law [Eq. (22)].

Substituting the Ampere's law Eq. (22) into electron momentum Eq. (30), we can derive the Ohm law equation for total vector potential A_{\parallel} . Subtracting Ohm's law for A_{\parallel} by Eq. (10) and using Eqs. (23)–(26), we can derive the equation for the non-adiabatic vector potential A_{\parallel}^{NA}

$$\left(\underbrace{\nabla_{\perp}^2}_{\{I\}} - \frac{\omega_{pe}^2}{c^2} \right) \frac{\partial A_{\parallel}^{NA}}{\partial t} = \frac{\omega_{pe}^2}{c^2} \chi_{\parallel} \underbrace{-c \nabla_{\perp}^2 (\mathbf{b}_0 \cdot \nabla \delta \phi_{ind})}_{\{II\}}, \quad (31)$$

where

$$\begin{aligned} \chi_{\parallel} = & \underbrace{-\frac{c}{en_0} \mathbf{b}_0 \cdot \nabla \delta P_{\parallel}^{NA}}_{\{III\}} - \underbrace{\frac{c}{en_0 B_0} \delta \mathbf{B}^{NA} \cdot \nabla P_{\parallel 0}}_{\{IV\}} - \underbrace{\frac{c}{en_0 B_0} \delta \mathbf{B} \cdot \nabla \delta P_{\parallel}^{NA}}_{\{V\}} - \underbrace{\frac{c}{B_0} \delta \mathbf{B} \cdot \nabla \delta \phi_{ind}}_{\{VI\}} \\ & + \underbrace{\frac{c}{B_0} \delta \mathbf{B} \cdot \nabla \langle \phi \rangle}_{\{VII\}} - \underbrace{\frac{cm_e}{en_0} \nabla \cdot [n_0 \delta u_{\parallel e} (3\mathbf{V}_c + \mathbf{V}_g) + n_0 u_{\parallel 0} \mathbf{V}_E]}_{\{VIII\}} - \underbrace{\frac{cm_e}{en_0} \nabla \cdot (n_0 \delta u_{\parallel e} \mathbf{V}_E)}_{\{IX\}} \\ & + \underbrace{\frac{c}{en_0} \frac{P_{\parallel 0} - P_{\perp 0}}{B_0^2} \delta \mathbf{B} \cdot \nabla B_0 + \frac{c}{en_0} \frac{\delta P_{\parallel}^{NA} - \delta P_{\perp}^{NA}}{B_0^2} \mathbf{B}_0 \cdot \nabla B_0}_{\{X\}}, \end{aligned}$$

We drop the ion contribution $\partial\delta\bar{u}_{i\parallel}/\partial t$ in Eq. (31) due to the small electron-to-ion mass ratio. In Eq. (31), terms {I} and {II} represent the electron inertia. Terms {III}, {IV}, and {V} are the pressure gradient terms associated with either the kinetic electron response or the non-adiabatic perturbed magnetic field. Term {VI} is the leading drive of the zonal current generated by drift Alfvén waves.⁵⁰ Term {VII} is the zonal flow effect on non-zonal current. Terms {VIII} and {IX} are linear and nonlinear convective motions, respectively. We compare the ordering of {IX} with {VI} as $O(\frac{IX}{VI}) \sim k_{\perp}^2 d_e^2$, and thus, term {IX} is as important as {VI} for the physics containing the $k_{\perp}^2 d_e^2 \sim 1$ scale such as the collisionless tearing mode. Term {X} represents the mirror force contribution. When we set $\delta P_{\parallel}^{NA} = \delta P_{\perp}^{NA} = 0$, i.e., removing the kinetic electron effects, Eq. (31) is equivalent to Eq. (7) from Liu and Chen,⁴¹ and this drift kinetic electron model reduces to the finite-mass fluid electron model.⁴¹ Equation (31) solves the non-adiabatic vector potential A_{\parallel}^{NA} from the non-adiabatic perturbed distribution δh . The perpendicular Laplacian on the left-hand-side can be ignored for long wavelength non-tearing modes. For the collisionless tearing mode, the wavelength is on the order of the electron skin depth anyway. Therefore, Eq. (31) is free from the cancellation problem.

Equations (1)–(3), (5), (9), (10)–(12), (15), (16), (18), (21)–(26), (28), (29), and (31) form a closed system for electromagnetic simulation with kinetic electrons. It can be seen that all the electron kinetic effects come into our system from the perturbed kinetic pressures, and the lower order moments are calculated from the moment equations, and thus, it guarantees the conservation properties of perturbed density and parallel flow through Eqs. (10), (21), (22), and (31) and the consistency between the electrostatic potential and vector potential (ion parallel flow contribution to the vector potential is much smaller than electron parallel flow). It will be shown that the perpendicular grid size does not need to resolve the electron skin depth when the wavelength is longer than the electron skin depth in the simulation of KAW in Sec. IV. The difference between the conservative scheme and fluid-kinetic hybrid electron model^{22–25} is that the fluid-kinetic hybrid electron model solves the electron drift kinetic equation approximately, while the conservative scheme solves the exact electron drift kinetic equation.

IV. VERIFICATION OF THE CONSERVATIVE SCHEME

To verify the conservative scheme for electromagnetic simulations with kinetic electrons, we have implemented it in the gyrokinetic toroidal code (GTC)⁷ and carried out simulations of the KAW in uniform plasmas and the collisionless tearing mode in the cylindrical geometry with magnetic shear. In this section, the quantities with subscript “e” represent the electron quantities.

A. Kinetic Alfvén wave in uniform plasmas

Assuming that the ion only provides the polarization density in uniform plasmas, we first use the conservative scheme to derive the linear dispersion relation. Equation (27) can be simplified in linear and uniform plasmas as

$$\left(\frac{\partial}{\partial t} + v_{\parallel}\mathbf{b}_0 \cdot \nabla\right)\delta h = -\frac{e}{m_e}\left(\mathbf{b}_0 \cdot \nabla\delta\phi + \frac{1}{c}\frac{\partial A_{\parallel}}{\partial t}\right)\frac{\partial f_{e0}}{\partial v_{\parallel}} - \left(\frac{\partial}{\partial t} + v_{\parallel}\mathbf{b}_0 \cdot \nabla\right)\delta f_a. \quad (32)$$

In the long wavelength limit, the gyrokinetic Poisson equation (5) reduces to

$$\frac{c^2}{4\pi eV_A^2}\nabla_{\perp}^2\delta\phi = \delta n_e. \quad (33)$$

In uniform plasmas, Eqs. (11), (18), (21), (22), and (31) reduce to

$$en_{e0}(\delta\phi + \delta\phi_{ind}) = \delta n_e T_{e0}, \quad (34)$$

$$\delta f_a = \frac{e(\delta\phi + \delta\phi_{ind})}{T_{e0}}f_{e0}, \quad (35)$$

$$\frac{\partial\delta n_e}{\partial t} + n_{e0}\mathbf{b}_0 \cdot \nabla\delta u_{\parallel e} = 0, \quad (36)$$

$$\delta u_{\parallel e} = \frac{c}{4\pi en_{e0}}\nabla_{\perp}^2 A_{\parallel}, \quad (37)$$

$$\left(\nabla_{\perp}^2 - \frac{\omega_{pe}^2}{c^2}\right)\frac{\partial A_{\parallel}^{NA}}{\partial t} = -c\nabla_{\perp}^2(\mathbf{b}_0 \cdot \nabla\delta\phi_{ind}) - \frac{\omega_{pe}^2}{en_{e0}c}\mathbf{b}_0 \cdot \nabla\delta P_{\parallel e}^{NA}. \quad (38)$$

Applying the Fourier transform to Eqs. (10) and (32)–(38) and considering $A_{\parallel} = \delta A_{\parallel}^A + A_{\parallel}^{NA}$: $\partial_t \rightarrow -i\omega$, $\mathbf{b}_0 \cdot \nabla \rightarrow ik_{\parallel}$, and $\nabla_{\perp} \rightarrow i\mathbf{k}_{\perp}$, the linear dispersion relation of KAW based on this model in the uniform plasmas is

$$\left(\frac{\omega^2}{k_{\parallel}^2 V_A^2} - 1\right)[1 + \xi_e Z(\xi_e)] = k_{\perp}^2 \rho_s^2, \quad (39)$$

where $\xi_e = \omega/\sqrt{2}k_{\parallel}v_{the}$, $\rho_s = C_s/\Omega_{ci}$, $v_{the} = \sqrt{T_{e0}/m_e}$, $C_s = \sqrt{T_{e0}/m_i}$, and $Z(\xi_e)$ is the plasma dispersion function: $Z(\xi_e) = \frac{1}{\sqrt{\pi}}\int_{-\infty}^{+\infty}\frac{e^{-t^2}}{t-\xi_e}dt$.

In the simulation of KAW in a uniform plasma, the electron temperature is $T_{e0} = 5.0$ keV, the magnetic field is $B_0 = 1.5$ T, and the ratio between parallel and perpendicular wave vectors is $k_{\parallel}/k_{\perp} = 0.01$. We scan the electron density and thus the value of $\beta_e = 8\pi n_{e0}T_{e0}/B_0^2$. First, we use $n_{e0} = 1.0 \times 10^{13}$ cm⁻³ and the corresponding $\beta_e = 0.9\%$ and verify the dependence of the frequency on the wavevector $k\rho_s$ and the perpendicular grid size $\Delta x/d_e$. The simulation results agree well with the analytic theory as shown in Fig. 1, which indicates that the perpendicular grid size can be much larger than the electron skin depth. Second, we fix the wavevector $k\rho_s = 0.48$, change the electron density from $n_{e0} = 1.0 \times 10^{13}$ cm⁻³ to $n_{e0} = 2.0 \times 10^{14}$ cm⁻³, and verify the dispersion relations of KAW for different β_e values. As shown in Fig. 2, both the frequency and damping rate agree with the analytic theory very well when $\beta_e \gg m_e/m_i$. In a high β_e regime, the damping of KAW is too weak to be measured accurately since the ion Landau damping is removed in the simulation.

These agreements between GTC simulations of the analytic theory verify that there is no constrain of the electron

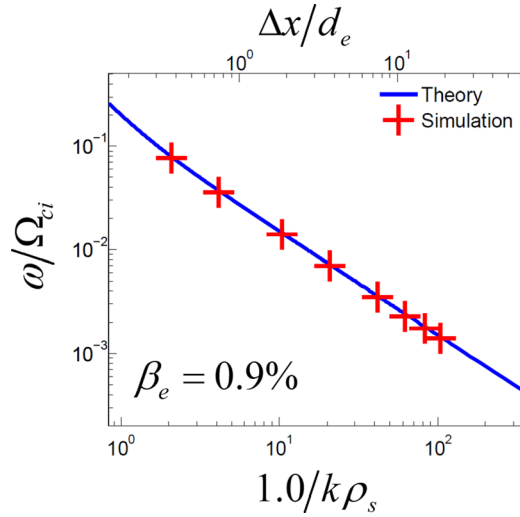


FIG. 1. Dependence of KAW frequency on the wavelength (bottom) and perpendicular grid size (top) from GTC simulations and from the analytic theory.

skin depth on the perpendicular grid size in our simulations. The simulations achieve high accuracy in both long wavelength and high β_e regimes, which demonstrates the numerical advantages of this model.

B. Collisionless tearing mode in cylindrical geometry

In this subsection, we verify the conservative scheme for the theory and simulation of the collisionless tearing mode in cylindrical geometry. For simplicity, we only keep the equilibrium current that drives the tearing mode and neglect the density and temperature gradients which could contribute to the real frequency of the tearing mode. Therefore, we would have a purely growing collisionless tearing mode. From Eqs. (10), (25), (32), (34), and (38), one can readily derive the electron response to the tearing mode,

$$\nabla_{\perp}^2 \omega A_{\parallel} = \frac{\omega_{pe}^2}{c} \left(\frac{1}{c} \omega A_{\parallel} - k_{\parallel} \delta \phi \right) \xi_e^2 Z'(\xi_e), \quad (40)$$

where $Z'(\xi_e)$ is the derivative of the plasma function with respect to ξ_e .

For the collisionless tearing mode in the plasmas with uniform density and temperature profiles but with the non-

uniform magnetic field, the continuity equation [Eq. (21)] reduces to

$$\frac{\partial \delta n_e}{\partial t} + n_{e0} \mathbf{b}_0 \cdot \nabla \delta u_{\parallel e} + n_{e0} \frac{\delta \mathbf{B}}{B_0} \cdot \nabla u_{\parallel e0} = 0, \quad (41)$$

where $u_{\parallel e0} = -\frac{c}{4\pi en_{e0}} \mathbf{b}_0 \cdot \nabla \times \mathbf{B}_0$ in the ion frame.

Combining Eqs. (33), (37), (40), and (41), one will have the eigenmode equation for the tearing mode,

$$\underbrace{\nabla_{\perp}^4 \omega^2 A_{\parallel}}_{\{\text{I}\}} = \underbrace{\nabla_{\perp}^2 \left[\frac{1}{d_e^2} \omega^2 \xi_e^2 Z'(\xi_e) A_{\parallel} \right]}_{\{\text{II}\}} - \underbrace{\frac{m_i}{m_e} k_{\parallel} \xi_e^2 Z'(\xi_e) (k_{\parallel} \nabla_{\perp}^2 - k_{\parallel}'') A_{\parallel}}_{\{\text{III}\}}, \quad (42)$$

where $k_{\parallel}'' = d^2 k_{\parallel} / dr^2$.

Following the asymptotic matching method of Drake and Lee⁵¹ and also Liu and Chen,⁴¹ one can derive the dispersion relation for the collisionless tearing mode. By noticing that in the inner region, near the mode rational surface $k_{\parallel} \sim 0$, the mode structure is steeper (i. e. $k_r \gg k_{\theta} \sim L_B$) than that of the outer ideal MHD region ($k_r \sim k_{\theta} \sim L_B$), so one only needs to keep the leading terms {I} and {II} in Eq. (42) for the inner region equation

$$\nabla_{\perp}^2 A_{\parallel i} = \frac{1}{d_e^2} \xi_e^2 Z'(\xi_e) A_{\parallel i}, \quad (43)$$

where the subscript “i” means the inner region.

For the outer ideal MHD region away from the mode rational surface, term {III} will dominate since the tearing mode frequency is smaller than the Alfvén wave frequency, so one can neglect the term {II} for the outer region. Since the magnetic diffusive time due to the electron inertial term {I} is much longer than the tearing mode and Alfvén wave periods, the electron inertia related term {I} can also be removed. Thus, the outer region equation for $A_{\parallel o}$ becomes

$$(k_{\parallel} \nabla_{\perp}^2 - k_{\parallel}'') A_{\parallel o} = 0, \quad (44)$$

where the subscript “o” means the outer region.

Using the constant A_{\parallel} approximation and matching the inner and outer regions by using the boundary condition, we get

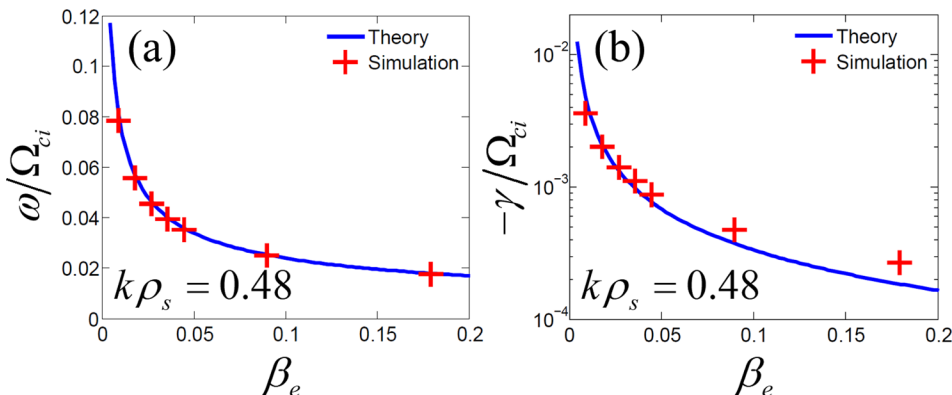
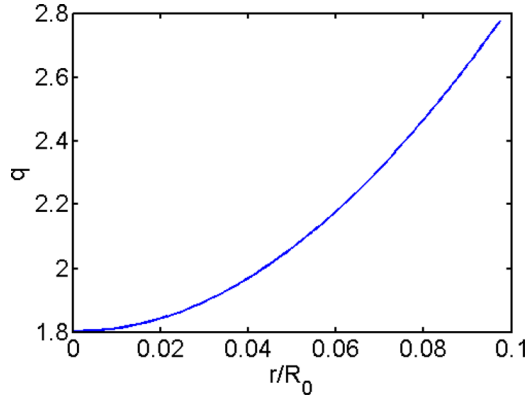


FIG. 2. Dependence of KAW frequency (a) and damping rate (b) on β_e from GTC simulations and from the analytic theory.

FIG. 3. Safety factor q profile in collisionless tearing mode simulation.

$$\frac{A_{||i}'}{A_{||i}} = \frac{A_{||o}'}{A_{||o}} = \Delta', \quad (45)$$

where $A_{||i}' = dA_{||i}/dr$, $A_{||o}' = dA_{||o}/dr$, and $\Delta' = d\Delta/dr$.

One will have the dispersion relation for the collisionless tearing mode from our kinetic model as

$$-i\omega = \gamma = \frac{d_e^2}{\sqrt{\pi}} |k'_{||} v_{te}| \Delta_o'. \quad (46)$$

The kinetic dispersion relation, Eq. (46), derived from our conservative scheme is the same as the result from the electron drift kinetic equation by Drake and Lee.⁵¹

When we set $\delta P_{||e}^{NA} = 0$ in Eq. (38), i.e., remove electron kinetic effects but keep finite electron inertia, we can get the growth rate of the collisionless tearing mode from the finite-mass electron fluid model:

$$-i\omega = \gamma = \frac{d_e^2}{\pi} |k'_{||} v_{te}| \Delta_o'. \quad (47)$$

This fluid dispersion relation, Eq. (47), is the same with the result of Liu and Chen's fluid model.⁴¹ The origin for the difference of $\sqrt{\pi}$ between Eqs. (46) and (47) comes from the fact that the finite mass electron fluid model assumes that the background electrons are two counter propagating cold beams with the same speed.⁴¹ In the kinetic model, we use the Maxwellian distribution for the background electron.⁵¹

After verifying the analytic dispersion relation of our formulation, we now verify the GTC simulation of the collisionless tearing mode using the conservative scheme. In order to compare with the analytic theory, we simulate the collisionless tearing mode in the cylindrical geometry with magnetic shear. The equilibrium parameters are uniform equilibrium electron density $n_{e0} = 1.0 \times 10^{12} \text{ cm}^{-3}$, temperature $T_{e0} = 5.0 \text{ keV}$, axial magnetic field $B_0 = 1.0 \text{ T}$, and axial length $L = 2\pi R_0$ where $R_0 = 1.0 \text{ m}$. It should be pointed out that the radial grid size in this collisionless tearing mode simulation needs to resolve the electron skin depth d_e near the rational surface since the mode structure of the collisionless tearing mode has a scale length of d_e . This is different from the KAW simulation in Sec. IV A, where the radial grid size does not need to resolve the d_e scale. In the cylindrical geometry, we carry out the simulations of the collisionless tearing mode in both fluid and kinetic regimes by using our model with the q profile as shown in Fig. 3, which gives rise to an unstable collisionless tearing mode with $m = 2$ and $n = 1$. First, we drop the second term on the RHS of Eq. (38), and our model reduces to the finite mass electron

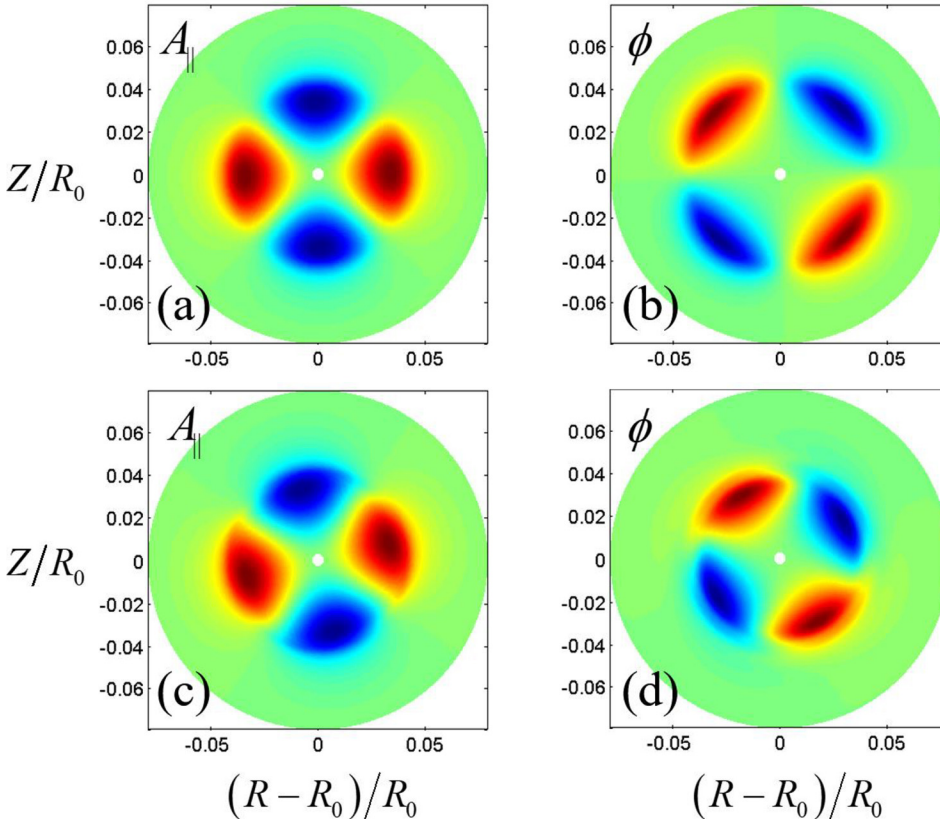


FIG. 4. Upper panels show the mode structures of (a) $A_{||}$ and (b) ϕ from GTC fluid electron simulations of the (2, 1) collisionless tearing mode in cylindrical geometry. Lower panels show mode structures of (c) $A_{||}$ and (d) ϕ from the corresponding GTC kinetic electron simulations.

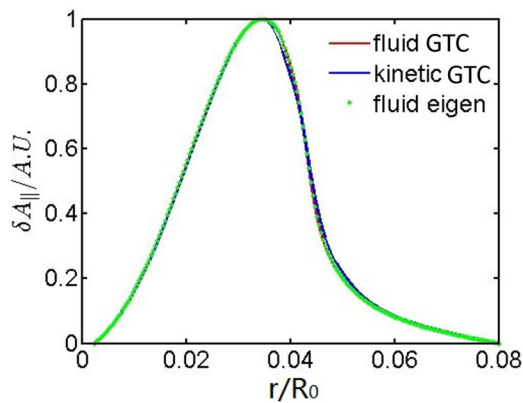


FIG. 5. Radial mode structures of A_{\parallel} in the (2, 1) collisionless tearing mode between GTC kinetic simulation, GTC fluid simulation, and fluid eigenvalue code in the cylindrical geometry.

fluid model.^{41,42} The fluid simulation with the realistic electron-ion mass ratio $m_e/m_i = 1/1837$ gives the growth rate $\gamma = 0.0014(C_s/R_0)$. The structures of this (2, 1) mode for the parallel vector potential A_{\parallel} and electrostatic potential ϕ on the poloidal plane are shown in Figs. 4(a) and 4(b). The fluid simulation results are verified by a 1D eigenvalue code⁴¹ solving the same fluid model, which gives the growth rate of $\gamma = 0.0015(C_s/R_0)$, and the mode structure agrees with the GTC fluid simulations. Second, we apply the exact equation (38) with the non-adiabatic pressure term in the kinetic electron simulation.

By using the same equilibrium parameter, the kinetic simulation gives the growth rate of the collisionless tearing mode $\gamma = 0.0031(C_s/R_0)$. The mode structures of the parallel vector potential A_{\parallel} and electrostatic potential ϕ on the poloidal plane are shown in Figs. 4(c) and 4(d). The analytic growth rate from the electron drift kinetic equation is estimated as $\gamma = 0.0027(C_s/R_0)$ by multiplying $\sqrt{\pi}$ to the fluid eigenvalue result according to Eqs. (46) and (47). GTC kinetic simulation results agree reasonably with the analytic theory. The small difference between the kinetic simulated and theoretical growth rate comes from the asymptotic method used in the analytic theory. The inner region is assumed to be infinitely narrow in the analytic theory but has a finite width in the simulation. Finally, Fig. 5 shows that radial mode structures of A_{\parallel} between the fluid eigenvalue code and GTC fluid simulation agree well and that kinetic electrons have little effects on the radial mode structure. Thus, our model can faithfully capture the physics of the collisionless tearing mode in both fluid and kinetic regimes.

V. CONCLUSIONS

In this paper, we present an efficient gyrokinetic ion and drift kinetic electron model for simulations of kinetic-MHD processes in the toroidal geometry. A novel conservative scheme is formulated for solving the electron drift kinetic equation. Both the vector potential and electron perturbed response are decomposed into adiabatic and non-adiabatic parts. The adiabatic parts of the vector potential and electron response are calculated analytically, while the non-adiabatic electron response is calculated by using the distribution function, and

the non-adiabatic vector potential is solved using the non-adiabatic electron response through Ohm's law, which helps to decrease the particle noise and mitigate the cancellation problem in the simulation. Only the kinetic pressures are calculated from the electron distribution function, while the lower order moments are calculated by using the moment equations, which guarantees the conservation properties of the electron perturbed density and parallel flow through the electron continuity equation and generalized Ohm's law. Thus, the consistency between the electrostatic potential and vector potential is enforced, which results in an accurate parallel electric field calculation.

Both the continuity equation and Ohm's law are derived by integrating the drift kinetic equation analytically, and the guiding center dynamics is described by the drift kinetic equation; thus, this new conservative scheme solves the exact drift kinetic equation for electrons. The dispersion relation of kinetic Alfvén waves in high β plasmas is verified in GTC simulation, which shows that the perpendicular grid size does not need to resolve the electron skin depth for the numerical accuracy and stability when the wavelength is longer than the electron skin depth. Finally, both the growth rate and mode structure of the collisionless tearing mode in GTC simulations are verified by the analytic theory and eigenvalue calculation. The applications of the conservative scheme for gyrokinetic simulations of kinetic-MHD processes ranging from the micro tearing mode to the neoclassical tearing mode in toroidal plasmas will be reported in the future.

We note that a mixed-variable algorithm proposed by Mishchenko *et al.*²¹ splits the vector potential into ideal MHD part and higher order perturbed part, where only the ideal MHD part is free from the cancellation problem. In contrast, our conservative scheme is generally free from the cancellation problem since the adiabatic vector potential (including the ideal MHD and adiabatic response associated with the parallel electric field and pressure gradients) is calculated from the adiabatic parallel electric field. Our scheme also enforces the consistency between the electrostatic potential and parallel vector potential by using the electron continuity equation, which leads to the accuracy of total parallel electric field calculation, and thus solves the numerical difficulty of electromagnetic simulation.⁴³

ACKNOWLEDGMENTS

We would like to thank W. W. Lee, L. Chen, W. M. Tang, Y. Chen, I. Holod, L. Shi, G. Dong, and Z. X. Lu for useful discussions. This work was supported by the U.S. Department of Energy (DOE) SciDAC GSEP Center and by the China National Magnetic Confinement Fusion Science Program (Grant Nos. 2013GB111001 and 2013GB111004). This work used resources of the Oak Ridge Leadership Computing Facility at the Oak Ridge National Laboratory (DOE Contract No. DE-AC05-00OR22725) and the National Energy Research Scientific Computing Center (DOE Contract No. DE-AC02-05CH11231).

¹T. C. Hender, J. C. Wesley, J. Bialek, A. Bondeson, A. H. Boozer, R. J. Buttery, A. Garofalo, T. P. Goodman, R. S. Granetz, Y. Gribov, O. Gruber, M. Gryaznevich, G. Giruzzi, S. Günter, N. Hayashi, P. Helander,

- C. C. Hegna, D. F. Howell, D. A. Humphreys, G. T. A. Huysmans, A. W. Hyatt, A. Isayama, S. C. Jardin, Y. Kawano, A. Kellman, C. Kessel, H. R. Koslowski, R. J. L. Haye, E. Lazzaro, Y. Q. Liu, V. Lukash, J. Manickam, S. Medvedev, V. Mertens, S. V. Mirnov, Y. Nakamura, G. Navratil, M. Okabayashi, T. Ozeki, R. Paccagnella, G. Pautasso, F. Porcelli, V. D. Pustovitov, V. Riccardo, M. Sato, O. Sauter, M. J. Schaffer, M. Shimada, P. Sonato, E. J. Strait, M. Sugihara, M. Takechi, A. D. Turnbull, E. Westerhof, D. G. Whyte, R. Yoshino, H. Zohm, and the ITPA MHD, Disruption and Magnetic Control Topical Group, *Nucl. Fusion* **47**, S128 (2007).
- ²A. J. Brizard and T. S. Hahm, *Rev. Mod. Phys.* **79**(2), 421 (2007).
- ³E. Frieman and L. Chen, *Phys. Fluids* **25**(3), 502–508 (1982).
- ⁴W. W. Lee, *Phys. Fluids* **26**, 556 (1983).
- ⁵W. W. Lee, *J. Comput. Phys.* **72**, 243 (1987).
- ⁶Z. Lin, T. S. Hahm, W. W. Lee, W. M. Tang, and R. B. White, *Science* **281**, 1835 (1998).
- ⁷A. M. Dimits, G. Bateman, M. A. Beer, B. I. Cohen, W. Dorland, G. W. Hammett, C. Kim, J. E. Kinsey, M. Kotschenreuther, A. H. Kritiz, L. L. Lao, J. Mandrekas, W. M. Nevins, S. E. Parker, A. J. Redd, D. E. Shumaker, R. Sydora, and J. Weiland, *Phys. Plasmas* **7**, 969 (2000).
- ⁸A. M. Dimits and W. W. Lee, *J. Comput. Phys.* **107**, 309 (1993).
- ⁹S. E. Parker and W. W. Lee, *Phys. Fluids B* **5**, 77 (1993).
- ¹⁰J. V. W. Reynders, Ph.D. thesis, Princeton University, 1992.
- ¹¹J. C. Cummings, Ph.D. thesis, Princeton University, 1995.
- ¹²I. Manuilskiy and W. W. Lee, *Phys. Plasmas* **7**, 1381 (2000).
- ¹³W. W. Lee, J. L. V. Lewandowski, T. S. Hahm, and Z. Lin, *Phys. Plasmas* **8**, 4435 (2001).
- ¹⁴Z. Lin, paper presented at the SciDAC Microturbulence Project Meeting, General Atomics, 2001.
- ¹⁵I. Holod and Z. Lin, *Phys. Plasmas* **20**, 032309 (2013).
- ¹⁶B. I. Cohen, A. M. Dimits, W. M. Nevins, Y. Chen, and S. Parker, *Phys. Plasmas* **9**, 251 (2002).
- ¹⁷J. Candy and R. E. Waltz, *J. Comput. Phys.* **186**, 545–581 (2003).
- ¹⁸Y. Chen and S. E. Parker, *J. Comput. Phys.* **189**, 463–475 (2003).
- ¹⁹R. Hatzky, A. Konies, and A. Mishchenko, *J. Comput. Phys.* **225**, 568–590 (2007).
- ²⁰Y. Chen and S. E. Parker, *Phys. Plasmas* **18**, 055703 (2011).
- ²¹A. Mishchenko, M. Cole, R. Kleiber, and A. Könies, *Phys. Plasmas* **21**, 052113 (2014).
- ²²Z. Lin and L. Chen, *Phys. Plasmas* **8**, 1447 (2001).
- ²³Y. Nishimura, Z. Lin, and W. X. Wang, *Phys. Plasmas* **14**, 042503 (2007).
- ²⁴I. Holod, W. L. Zhang, Y. Xiao, and Z. Lin, *Phys. Plasmas* **16**, 122307 (2009).
- ²⁵W. Deng, Z. Lin, and I. Holod, *Nucl. Fusion* **52**, 023005 (2012).
- ²⁶E. A. Startsev and W. W. Lee, *Phys. Plasmas* **21**, 022505 (2014).
- ²⁷L. Villard, S. J. Allfrey, A. Bottino, M. Brunetti, G. L. Falchetto, V. Grandgirard, R. Hatzky, J. Nührenberg, A. G. Peeters, O. Sauter, S. Sorge, and J. Vaclavik, *Nucl. Fusion* **44**(1), 172 (2004).
- ²⁸A. Bottino, T. Vernay, B. Scott, S. Brunner, R. Hatzky, S. Jolliet, B. F. McMillan, T. M. Tran, and L. Villard, *Plasma Phys. Controlled Fusion* **53**(12), 124027 (2011).
- ²⁹Z. Lin, Y. Nishimura, Y. Xiao, I. Holod, W. L. Zhang, and L. Chen, *Plasma Phys. Controlled Fusion* **49**, B163 (2007).
- ³⁰Y. Xiao and Z. Lin, *Phys. Rev. Lett.* **103**, 085004 (2009).
- ³¹W. Deng, Z. Lin, I. Holod, Z. Wang, Y. Xiao, and H. Zhang, *Nucl. Fusion* **52**, 043006 (2012).
- ³²Z. Wang, Z. Lin, I. Holod, W. W. Heidbrink, B. Tobias, M. Van Zeeland, and M. E. Austin, *Phys. Rev. Lett.* **111**, 145003 (2013).
- ³³I. Holod and Z. Lin, *Plasma Phys. Controlled Fusion* **52**, 035002 (2010).
- ³⁴H. Zhang and Z. Lin, *Phys. Plasmas* **17**, 072502 (2010).
- ³⁵Y. Xiao and Z. Lin, *Phys. Plasmas* **18**, 110703 (2011).
- ³⁶Y. Xiao, I. Holod, Z. X. Wang, Z. Lin, and T. G. Zhang, *Phys. Plasmas* **22**, 022516 (2015).
- ³⁷I. Holod, D. Fulton, and Z. Lin, *Nucl. Fusion* **55**, 093020 (2015).
- ³⁸X. Liao, Z. Lin, I. Holod, Y. Xiao, B. Li, and P. B. Snyder, *Phys. Plasmas* **23**, 122507 (2016).
- ³⁹H. S. Xie, Y. Xiao, and Z. Lin, *Phys. Rev. Lett.* **118**, 095001 (2017).
- ⁴⁰D. Liu, W. Zhang, J. McClenaghan, J. Wang, and Z. Lin, *Phys. Plasmas* **21**, 122520 (2014).
- ⁴¹D. Liu and L. Chen, *Plasma Phys. Controlled Fusion* **53**, 062002 (2011).
- ⁴²D. Liu, J. Bao, T. Han, J. Wang, and Z. Lin, *Phys. Plasmas* **23**, 022502 (2016).
- ⁴³J. Bao, Z. Lin, and Z. X. Lu, “A conservative scheme for electromagnetic simulation of magnetized plasmas with kinetic electrons” (submitted); pre-print [arXiv:1702.01406](https://arxiv.org/abs/1702.01406).
- ⁴⁴A. M. Dimits, *Phys. Plasmas* **19**, 022504 (2012).
- ⁴⁵J. F. Drake, N. T. Gladd, C. S. Liu, and C. L. Chang, *Phys. Rev. Lett.* **44**, 994 (1980).
- ⁴⁶G. Dong, J. Bao, A. Bhattacharjee, A. Brizard, Z. Lin, and P. Porazik, *Phys. Plasmas* **24**, 081205 (2017).
- ⁴⁷F. L. Hinton and R. D. Hazeltine, *Rev. Mod. Phys.* **48**, 239 (1976).
- ⁴⁸Z. Lin, W. M. Tang, and W. W. Lee, *Phys. Plasmas* **2**, 2975 (1995).
- ⁴⁹Z. Lin, W. M. Tang, and W. W. Lee, *Phys. Rev. Lett.* **78**, 456 (1997).
- ⁵⁰L. Chen and F. Zonca, *Rev. Mod. Phys.* **88**, 015008 (2016).
- ⁵¹J. F. Drake and Y. C. Lee, *Phys. Fluids* **20**, 1341–1353 (1977).
- ⁵²W. W. Lee and H. Qin, *Phys. Plasmas* **10**, 3196 (2003).